STC1 promotes osteogenic differentiation and represses inflammation via inhibition of NF-κB signaling in mesenchymal stromal cells

CHEN YANG[1*], XIN LI[1*], PENG WANG[1], YITONG CHEN[1], ERLI WU[1], QIAN CHEN[1], JING HU[1], FU ZHENG[1], LAMU GONGSANG[2], JIAYU LI[2], MENGYUAN ZHANG[1], JING ZHOU[1], BING HAN[3], AMR A. BADRELDIN[3], YUKA MIYAMOTO[4], JIN KOO KIM[5], INSOON CHANG[4], JIA CHANG[3], PAUL H. KREBSBACH[5], LIYUAN HUANG[1], XIAOPING XU[6], XIAOYAN CHEN[1], PENG DENG[1], QIANMING CHEN[1] and LIJIE FAN[1]

[1]Key Laboratory of Oral Biomedical Research of Zhejiang Province, School of Stomatology, Zhejiang University School of Medicine, Engineering Research Center of Oral Biomaterials and Devices of Zhejiang Province, Zhejiang Provincial Clinical Research Center for Oral Diseases, Stomatology Hospital, Hangzhou, Zhejiang 310000, P.R. China; [2]School of Stomatology, Zhejiang University School of Medicine, Hangzhou, Zhejiang 310058, P.R. China; [3]Section of Periodontics, Division of Regenerative and Reconstructive Sciences, School of Dentistry, University of California, Los Angeles, Los Angeles, CA 90095, USA; [4]Section of Endodontics, Division of Regenerative and Reconstructive Sciences, School of Dentistry, University of California, Los Angeles, Los Angeles, CA 90095, USA; [5]Division of Oral and Systemic Health Sciences, School of Dentistry, University of California, Los Angeles, Los Angeles, CA 90095, USA; [6]State Key Laboratory of Oral Diseases and National Center for Stomatology and National Clinical Research Center for Oral Diseases and Research Unit of Oral Carcinogenesis and Management and Chinese Academy of Medical Sciences, West China Hospital of Stomatology, Sichuan University, Chengdu, Sichuan 610041, P.R. China

Received February 12, 2026; Accepted June 17, 2026

DOI: 10.3892/mmr.2026.13983

Abstract. The aging of mesenchymal stromal cells (MSCs) is characterized by impaired osteogenic differentiation and enhanced adipogenic differentiation. Studies have identified stanniocalcin-1 (STC1) as a core component of the senescence-associated secretory phenotype and a regulator of osteoblast maturation; however, its role in MSC biology remains poorly understood. In the present study, bone marrow-derived MSCs were used and *in vitro* functional assays together with molecular and omics-based analyses were performed to investigate the role of STC1. It was observed that STC1 expression was upregulated in aged MSCs and during both osteogenic and adipogenic differentiation. Small interfering RNA-mediated depletion of STC1 reduced cellular senescence and notably impaired osteogenic differentiation, whereas adipogenic and chondrogenic differentiation were not significantly affected. RNA sequencing revealed that *STC1* knockdown led to the downregulation of osteogenesis-related genes and the concomitant upregulation of inflammatory factors. Genes associated with closing differentially accessible regions (DARs) were enriched in osteogenic pathways, whereas those associated with opening DARs were predominantly involved in inflammatory responses. Mechanistically, *STC1* knockdown led to the activation of NF-κB signaling. Pharmacological inhibition assays using NF-κB inhibitors were performed to validate pathway involvement. Pharmacological inhibition of NF-κB signaling significantly mitigated the impairment in osteogenic differentiation and attenuated the inflammatory response induced by STC1 depletion. Collectively, these findings suggest that STC1 is involved in the regulation of osteogenic differentiation and inflammatory signaling through the modulation of NF-κB activity in MSCs. Furthermore, targeting STC1 while inhibiting NF-κB signaling may represent a promising therapeutic strategy for alleviating MSC dysfunction and age-related bone loss.

Correspondence to: Professor Qianming Chen or Professor Lijie Fan, Key Laboratory of Oral Biomedical Research of Zhejiang Province, School of Stomatology, Zhejiang University School of Medicine, Engineering Research Center of Oral Biomaterials and Devices of Zhejiang Province, Zhejiang Provincial Clinical Research Center for Oral Diseases, Stomatology Hospital, 166 North Qiutao Road, Shangcheng, Hangzhou, Zhejiang 310000, P.R. China
E-mail: qmchen@zju.edu.cn
E-mail: ddmm55@zju.edu.cn

*Contributed equally

Abbreviations: MSCs, mesenchymal stromal cells; STC1, stanniocalcin-1; SASP, senescence-associated secretory phenotype; DARs, differentially accessible regions; ROS, reactive oxygen species

Key words: STC1, MSCs, osteogenesis, senescence, NF-κB, inflammation

Introduction

Mesenchymal stromal cells (MSCs) are multipotent cells that play notable roles in tissue homeostasis and regeneration (1,2);

however, MSCs undergo cellular senescence during aging. In addition to a decline in cell population, aged MSCs are associated with impaired osteogenic differentiation and enhanced adipogenic differentiation (3-5). This imbalance between osteogenesis and adipogenesis is associated with the development of age-related bone loss and metabolic disorders. Aged MSCs also secrete pro-inflammatory cytokines, growth factors and extracellular matrix-remodeling proteins, collectively known as the senescence-associated secretory phenotype (SASP), which creates a hostile microenvironment that inhibits osteogenesis and promotes adipogenesis (6,7).

Cellular senescence is driven by a variety of intrinsic and extrinsic factors. Oxidative stress, particularly reactive oxygen species (ROS), is a key driver of senescence. As cells age, ROS levels increase, leading to DNA damage, protein modifications and lipid peroxidation (8,9). This damage activates DNA repair mechanisms, ultimately leading to cell cycle arrest and senescence (10). In addition, aging is often associated with a persistent inflammatory state (11,12). This chronic low-grade inflammation may be attributed to genomic instability, including expression of retrotransposable elements, telomere attrition and epigenetic alterations (13-15). Ultimately, inflammatory factors, such as SASP, further promote cellular senescence (7).

Stanniocalcin-1 (STC1) was originally identified as a glycoprotein hormone secreted by the corpuscles of Stannius in teleost fish, where it regulates phosphate and calcium homeostasis (16). More recently, STC1 has been identified as a core component of the SASP factors (17); however, its effects on inflammation appear to be tissue-specific and cell-type dependent. For example, STC1 exhibits a protective effect by suppressing the inflammatory cascade in lipopolysaccharide-induced lung injury. However, STC1 also mediates oxidative stress-induced parthanatos, a form of programmed cell death, and amplifies inflammation in dextran sulfate sodium-induced colitis (18).

Furthermore, STC1 is expressed in bone tissue, including osteoblasts and chondrocytes (19). Transgenic mice overexpressing *STC1* show a marked decrease in birth weight and reduced adult body size, possibly owing to the inhibitory effects of additional STC1 on longitudinal bone growth at the growth plate (20-22). However, the role of STC1 in the regulation of osteogenesis remains under debate. Yoshiko *et al* (23) reported that STC1 stimulated the maturation of osteoblasts derived from rat calvaria bone, whereas Kim *et al* (24) observed that STC1 inhibited BMP2-induced osteoblast differentiation. Notably, these discrepancies may reflect the cell type- and differentiation stage-dependent functions of STC1 in skeletal lineage cells. In addition to its roles in differentiated skeletal cells, emerging evidence suggests that STC1 also participates in the regulation of MSC function. Previous studies have shown that MSC-derived STC1 exerts anti-inflammatory, cytoprotective and ROS-regulatory effects in multiple disease models, including *in vivo* mouse pulmonary fibrosis and zymosan-induced peritonitis models, *in vitro* oxidative damage models of lung epithelial cells, UV-irradiated fibroblasts and NLRP3 inflammasome-activated macrophages (25-28). STC1 secretion by MSCs is responsive to cellular stress and mechanotransduction signals and has been implicated in immunomodulatory adaptation and maintenance of cellular homeostasis (25,26). Moreover, inhibition of STC1 in tonsil-derived MSCs was reported to increase intracellular ROS levels and impair MSC proliferative capacity, supporting a role for STC1 in MSC stress regulation (27). Nevertheless, the role of STC1 in MSC senescence and early differentiation remains unclear. In the present study, it was demonstrated that *STC1* knockdown inhibited MSC senescence and its effect on differentiation and inflammatory response in MSCs were further investigated. The present study aimed to determine whether STC1 regulates MSC senescence and to define its functional roles in osteogenic or adipogenic differentiation and inflammatory responses. STC1 knockdown was used to assess its effects on these processes in MSCs.

Materials and methods

Mice. All animal procedures were approved by the Institutional Animal Care and Use Committee of Zhejiang University (approval nos. ZJU20230513 and ZJU20240033) and were conducted in accordance with institutional guidelines and the ARRIVE recommendations. A total of 40 mice were used in the present study. Animals were purchased from Laboratory Animal Center of Zhejiang University and housed under specific pathogen-free (SPF) conditions at 22±2˚C with 50±10% relative humidity under a 12-h light/dark cycle, with free access to standard chow and water. Animals were monitored daily for general health status, including body condition, activity, grooming behavior, food and water intake and signs of pain or distress. Humane endpoints were predefined as follows: Body weight loss of 20-25% or evidence of cachexia and wasting syndrome; complete anorexia for 24 h; partial anorexia (<50% of normal caloric intake) for 3 consecutive days; and inability or extreme reluctance to stand or inability to obtain food or water, persisting for 24 h in the absence of anesthesia or analgesia. No animals were found dead prior to scheduled euthanasia or reached the predefined humane endpoints during the study. No longitudinal *in vivo* intervention was performed in the present study. Animals were euthanized immediately prior to tissue collection for MSC isolation, and all tissue collection procedures were completed within the same day. Animals were euthanized by gradual-fill CO_2 inhalation at a flow rate of 30% of the chamber volume per minute, followed by cervical dislocation. Death was confirmed by the absence of heartbeat and respiration together with loss of corneal and pedal reflexes before tissue collection. The mice used in the present study were male and female in equal proportions, including both young (8 weeks old, weighing 20-25 g) and aged (20 months old, weighing 35-45 g) at the time of experiments.

Cell culture. MSCs were isolated from the femora and tibiae of young (2-month-old) and aged (20-month-old) C57BL/6 mice via flushing and were cultured in Dulbecco's Modified Eagle Medium high glucose (4.5 g/l) (DMEM high glucose (4.5 g/l); Gibco; Thermo Fisher Scientific, Inc.) supplemented with 10% FBS (Gibco; Thermo Fisher Scientific, Inc.) and 1% penicillin/streptomycin (Gibco; Thermo Fisher Scientific, Inc.) at 37˚C within a 5% CO_2 incubator. After 7-10 days of culture, the cells were passaged using 0.25% trypsin (Gibco; Thermo Fisher Scientific, Inc.). BAY 11-7082 (1 and 2 μM), JSH-23

Table I. Related to methods, the sequences of primers used in the present study.

Gene	Application	Forward primer sequences	Reverse primer sequences
si-*Scr*	Transfection	UUCUCCGAACGUGUCACGUTT	ACGUGACACGUUCGGAGAATT
si-*Stc1*-1	Transfection	CGGUCAGUACAAUCAGAGA	UCUCUGAUUGUACUGACCG
si-*Stc1*-2	Transfection	CUUGUACAGUGCUGCUAAA	UUUAGCAGCACUGUACAAG
Stc1	RT-qPCR	AGGAGGACTGCTACAGCAAGCT	TCCAGAAGGCTTCGGACAAGTC
Alp	RT-qPCR	CCAGAAAGACACCTTGACTGTGG	TCTTGTCCGTGTCGCTCACCAT
Ibsp	RT-qPCR	ACAATCCGTGCCACTCACTC	CCGGTACTTAAAGACCCCGTT
Ocn	RT-qPCR	GGACCATCTTTCTGCTCACTCTGC	TCCTGCTTGGACATGAAGGCTTTG
Adipoq	RT-qPCR	GTTGCAAGCTCTCCTGTTCC	ATCCAACCTGCACAAGTTCC
Cebpα	RT-qPCR	ACTCCTCCTTTTCCTACCG	AGGAAGCAGGAATCCTCC
Lpl	RT-qPCR	GGGAGTTTGGCTCCAGAGTTT	TGTGTCTTCAGGGGTCCTTAG
Sox9	RT-qPCR	CGGAACAGACTCACATCTCTCC	GCTTGCACGTCGGTTTTGG
Col2a1	RT-qPCR	CCTCAAGGCAAAGTTGGTCCT	CTCCCGTCTCACCGTCTTTT
Il-1α	RT-qPCR	GAGAGCCGGGTGACAGTATC	TGACAAACTTCTGCCTGACG
Tnf-α	RT-qPCR	CCTGTAGCCCACGTCGTAG	GGGAGTAGACAAGGTACAACCC
β-actin	RT-qPCR	CATTGCTGACAGGATGCAGAAGG	TGCTGGAAGGTGGACAGTGAGG

RT-qPCR, reverse transcription-quantitative PCR; si, small interfering RNA.

(20 and 50 μM) and vehicle controls were added to media as indicated. After 24 h of treatment, the culture medium was refreshed.

RNA interference. To knock down STC1 in MSCs, *Stc1* small interfering RNAs (siRNAs; si-*Stc1*) or scrambled siRNAs (si-*Scr*) were transfected into MSCs using Lipofectamine® RNAiMax reagent (Thermo Fisher Scientific, Inc.). Specifically, siRNAs (final concentration; 50 nM) and Lipofectamine® RNAiMax were diluted separately in Opti-MEM medium (Gibco; Thermo Fisher Scientific, Inc.), combined and then incubated at room temperature for 10 min to induce complex formation. The transfection mixture was added directly to the cell culture medium. The transfection was performed at 37˚C in a 5% CO_2 incubator for 6 h, after which the medium was replaced with fresh complete medium, and subsequent experiments were conducted 48 h after transfection. Table I lists the siRNA sequences.

Alkaline phosphatase (ALP), alizarin red S (ARS), Oil red O and alcian blue staining. Osteogenic and adipogenic differentiation of MSCs was conducted as previously described (29,30). Briefly, osteogenic differentiation was induced by culturing MSCs in osteogenic induction medium consisting of 100 μM ascorbic acid (MilliporeSigma), 2 mM β-glycerophosphate (MilliporeSigma), and 10^{-7} M dexamethasone (MilliporeSigma). Adipogenic differentiation was induced using adipogenic induction medium containing 1 μM dexamethasone (MilliporeSigma), 10 μg/ml insulin (MilliporeSigma), 0.5 mM 3-isobutyl-1-methylxanthine (MilliporeSigma), and 0.2 mM indomethacin (MilliporeSigma). For chondrogenic induction, the inducing media were prepared using DMEM high glucose (4.5 g/l) supplemented with 10^{-7} M dexamethasone (MilliporeSigma), 1 μM ascorbate-2-phosphate (MilliporeSigma) and 10 ng/ml transforming growth factor-b1 (ABclonal Biotech Co., Ltd.), along with 10% FBS and 1% penicillin/streptomycin.

For ALP staining, osteogenic induction medium was added for 1 week (with the medium refreshed every 3 days), until >70% confluency was confirmed. Cells were fixed using 70% ethanol at room temperature for 15 min and incubated with ALP staining solution (Beyotime Biotechnology) at 37˚C in the dark for 5 min. Images were acquired using a CanoScan LiDE 110 scanner (Canon, Inc.). For quantification of ALP activity, cell lysates were prepared in RIPA buffer (without protease/phosphatase inhibitors; Beyotime Biotechnology) and centrifuged at 10,000 x g at 4˚C for 5 min. The resulting supernatants were analyzed using an ALP assay kit (Beyotime Biotechnology) according to the manufacturer's instructions. ALP activity was normalized to the total protein concentration of each lysate, as determined using a bicinchoninic acid (BCA) protein assay kit (Beyotime Biotechnology).

For ARS staining, osteogenic induction medium was added for 3 weeks (with the medium refreshed every 3 days), until >70% confluency was confirmed. Cells were fixed using 70% ethanol at room temperature for 1 h and stained using 1% ARS solution (MilliporeSigma) at room temperature for 30 min. For quantification, the plate was destained using 10% cetylpyridinium chloride solution (MilliporeSigma), and optical density was measured at 562 nm.

For Oil Red O staining, adipogenic induction medium was added for 1 week (with the medium refreshed every 3 days), until >90% confluency was confirmed. Cells were fixed using 70% at room temperature ethanol for 10 min and then stained using Oil Red O working solution at room temperature for 5 min. After removal of the staining solution, the cells were rinsed twice using double distilled H_2O. The plate was air-dried, and the stained lipid droplets were eluted in isopropanol. Absorbance was measured at 450 nm using a microplate reader (Omega Bio-Tek, Inc.) to quantify lipid accumulation.

For Alcian blue staining, chondrogenic induction medium (prepared as aforementioned in this section) was added for 3-4 weeks (with the medium refreshed every 3 days), until >90% confluency was confirmed. Cells were fixed using 4% paraformaldehyde at room temperature for 15 min and then stained with Alcian blue solution (MilliporeSigma) for at room temperature 30 min. After image acquisition using the aforementioned scanner, stained Alcian blue was extracted using 6 M guanidine hydrochloride for 6 h at room temperature. Absorbance was measured at 630 nm.

Senescence associate β-galactosidase (SA-β-Gal) staining. SA-β-Gal staining was performed following previously published procedures (29,31). Cells were fixed using a freshly prepared solution containing 2% formaldehyde and 0.2% glutaraldehyde for 5 min at room temperature. After fixation, the cells were rinsed twice using PBS and incubated with X-gal staining solution (containing 1 mg/ml X-gal (Shanghai Macklin Biochemical Co., Ltd.), 5 mM potassium ferricyanide (Shanghai Macklin Biochemical Co., Ltd.), 5 mM potassium ferrocyanide (Shanghai Macklin Biochemical Co., Ltd.), 150 mM NaCl (Shanghai Macklin Biochemical Co., Ltd.) and 2 mM $MgCl_2$ (Shanghai Macklin Biochemical Co., Ltd.) in a pH 6.0 buffer system) at 37˚C in the dark for 6-8 h. Images were captured under a bright-field microscope (Leica Microsystems GmbH) from five randomly selected fields per sample. SA-β-Gal-positive cells were quantified as the percentage of blue stained cells among the total number of cells and statistically analyzed.

Cell counting kit (CCK)-8 assay. Cells were seeded in 96-well plates at a density of $1x10^4$ cells per well. On days 1, 3 and 5 after seeding, CCK-8 reagent (Beyotime Biotechnology) was added to each well according to the manufacturer's instructions. Afterward, the plates were incubated to allow the reagent to react with the cells. After 2 h of incubation at 37˚C, absorbance was measured at 450 nm.

Reverse transcription-quantitative (q)PCR analysis. Total RNA was extracted using TRIzol™ reagent (Invitrogen; Thermo Fisher Scientific, Inc.), and 1 μg aliquots of RNA were transcribed to cDNA using reverse transcriptase (Vazyme Biotech Co., Ltd.) at 50˚C for 10 min followed by 85˚C for 10 sec. Afterward, qPCR was performed using an SYBR Green PCR kit (Vazyme Biotech Co., Ltd.) on a QuantStudio™ 7 Flex System (Applied Biosystems; Thermo Fisher Scientific, Inc.). PCR cycling involved initial denaturation at 95˚C for 5 min, followed by 40 cycles of denaturation at 95˚C for 30 sec, annealing at 60˚C for 30 sec and extension at 72˚C for 30 sec. Relative gene expression was normalized to *β-actin* and analyzed via the $2^{-\Delta\Delta Cq}$ method (32). Table I contains the primer sequences.

Western blot analysis. Total cellular protein was extracted using RIPA lysis buffer (Beyotime Biotechnology) on ice. Protein concentration in the lysates was determined using a BCA assay kit according to the manufacturer's instructions. Aliquots of the lysates were separated via 10% SDS-PAGE and subsequently transferred onto a PVDF membrane. A total of 20-30 μg of protein per lane was loaded. The membrane was blocked using 5% BSA (Beyotime Biotechnology) in TBST (Tris-buffered saline containing 0.1% Tween-20) for 1 h at room temperature, followed by incubation with specific primary antibodies overnight at 4˚C. After washing with TBST, the membrane was incubated with HRP-conjugated secondary antibodies for 1 h at room temperature. Protein bands were visualized using an enhanced chemiluminescence substrate (Beyotime Biotechnology) and recorded using a chemiluminescence imaging system (Bio-Rad Laboratories, Inc.). The following antibodies were used: Rabbit anti-NF-κB p65 (1:1,000; cat. no. A19653; ABclonal Biotech Co., Ltd.), rabbit anti-phospho-NF-κB p65 (1:1,000; cat. no. AP0124; ABclonal Biotech Co., Ltd.), rabbit anti-IκBα (1:1,000; cat. no. A19714; ABclonal Biotech Co., Ltd.), rabbit anti-phospho-IκBα (1:1,000; cat. no. AP0707; ABclonal Biotech Co., Ltd.), rabbit anti-β-Actin (1:50,000; cat. no. AC050; ABclonal Biotech Co., Ltd.) and HRP-conjugated goat anti-rabbit IgG (1:70,000; cat. no. HA1001; HUABIO).

RNA-sequencing library construction and analysis. Total RNA was isolated using TRIzol reagent. Library construction and RNA sequencing were performed at Shanghai OE Biomedical Technology Co., Ltd. RNA libraries were prepared using VAHTS Universal V10 RNA-seq Library Prep Kit (cat. no. NR616-01; Vazyme Biotech Co., Ltd.) according to the manufacturer's instructions. Subsequently, the FASTQ files of raw paired-end RNA-seq reads were mapped to the mouse reference genome NCBI38/mm10 using STAR (version 2.7.11a; https://github.com/alexdobin/STAR). The mapped reads were then quantified to generate raw counts using featureCounts (version 2.0.3) (33,34). Principal component analysis (PCA) was performed, and significantly differentially expressed genes (DEGs) (si-*Stc1* versus si-*Scr*) were identified using the DESeq2 package (version 1.48.2; https://github.com/thelovelab/DESeq2) in R (4.5.1; RStudio, Inc.), with a threshold $P<0.05$ and fold changes of >1.5. Heatmaps of the relative expression of representative genes were further generated using the Complexheatmap package (version 2.24.1; https://github.com/jokergoo/ComplexHeatmap) in R.

The gene expression omnibus (GEO) dataset (accession GSE113253, https://www.ncbi.nlm.nih.gov/geo/query/acc.cgi?acc=GSE113253,https://pubmed.ncbi.nlm.nih.gov/30833796/), originally reported by Rauch *et al* (35), comprises transcriptional profiles of primary MSCs at multiple time points (0 days, 4 h, 1 day, 3 days and 7 days) during osteoblast and adipocyte differentiation (36). Raw expression matrices were downloaded from GEO and processed in R (version 4.3.1). DEGs were identified using DESeq2 and subsequently subjected to K-means clustering analysis. Read counts were normalized to transcripts per million to facilitate downstream downstream analyses. Gene set enrichment analysis (GSEA) was performed using the R package clusterProfiler (version 4.10.0, https://bioconductor.org/packages/clusterProfiler/) based on Hallmark and KEGG gene sets obtained from the Molecular Signatures Database (https://www.gsea-msigdb.org/gsea/msigdb).

Assay for transposase-accessible chromatin (ATAC)-sequencing library construction and analysis. The ATAC-sequencing library was constructed using a Hyperactive

ATAC-seq Library Prep Kit (Vazyme Biotech Co., Ltd.) according to the manufacturer's instructions. Specifically, nuclei were isolated from 50,000 cells via incubation on ice for 5 min, followed by centrifugation at 500 x g at 4˚C. Tagmentation was performed at 37˚C for 30 min. After purification, DNA fragments were amplified using PCR enzymes and indexed primers (Vazyme Biotech Co., Ltd.). Size selection was performed using ATAC DNA Clean Beads (Vazyme Biotech Co., Ltd.), and libraries were sequenced on the Illumina Xplus platform (Illumina, Inc.) using PE150. Raw ATAC-seq read FASTQ files were first processed using Trim Galore (version 0.6.10; https://github.com/FelixKrueger/TrimGalore) to remove the adaptors and were then aligned to NCBI38/mm10 mouse reference genome using Bowtie2 (version 2.4.4-1) (37). Uniquely mapped reads were retained for peak calling using MACS2 with a significance threshold of P<0.05 (38). To generate a consensus set of unique peaks across all samples, read counts within these peak regions were quantified using featureCounts. Differentially accessible regions (DARs) were identified using the DESeq2 package in R, with a P<0.05 and fold change of >1.5. Subsequently, the ChIPseeker package in R (version 1.44.0; https://github.com/YuLab-SMU/ChIPseeker) in R was used to identify the nearest genes, with the transcription start site region defined as -3 kb to +3 kb.

Statistical analysis. Data are presented as the mean ± standard deviation. Data analysis was conducted using GraphPad Prism 10.0 software (Dotmatics). Differences between groups were assessed using unpaired t-tests, one-way ANOVA (with Dunnett's post hoc test) or two-way ANOVA (with Tukey's post hoc test). P<0.05 was considered to indicate a statistically significantly difference.

Results

Stc1 upregulation during cellular senescence and osteogenic and adipogenic differentiation of MSCs. Considering that STC1 has been reported to be upregulated in multiple aged tissues, its expression levels during MSC senescence were first examined (17), and MSCs were isolated from 2- and 20-month-old mice. As hypothesized, MSCs from 20-month-old mice exhibited significantly higher *Stc1* expression than those from 2-month-old mice (Fig. S1A). Next, publicly available sequencing data (GEO: GSE113253) on osteogenic and adipogenic differentiation of MSCs was analyzed. Gene clustering analysis revealed multiple modules with distinct temporal expression patterns during MSC differentiation into osteoblasts and adipocytes (Fig. 1A). Specifically, the C1 and C2 modules captured gene expression changes associated with osteogenic differentiation. Functional enrichment analysis revealed that these modules were significantly associated with osteogenesis-related biological processes, including 'ossification', the 'canonical Wnt signaling pathway' and 'bone development'. By contrast, the C3 and C4 modules represented gene expression programs associated with adipogenic differentiation and were enriched in 'fatty acid metabolic process', reflecting commitment to the adipocyte lineage. Consistent with these findings, GSEA demonstrated that osteoblast-related signaling pathways were significantly activated during osteogenic differentiation (Fig. 1B), whereas adipogenesis-related pathways were robustly enriched during adipogenic differentiation (Fig. 1C). Collectively, these results highlighted the stage-specific transcriptional programs underlying MSC lineage specification into osteoblasts and adipocytes. Furthermore, the temporal expression dynamics of *Stc1* during MSC differentiation were examined. During osteogenic induction, *Stc1* expression exhibited marked temporal variation, with notably higher levels observed at days 3 and 14 (Fig. 1D). By contrast, *Stc1* expression exhibited a continuous upward trend throughout adipogenic differentiation (Fig. 1E). These observations indicated that *Stc1* was dynamically regulated during MSC lineage commitment and might participate in both osteogenic and adipogenic differentiation processes. To further validate the upregulation of *Stc1*, mRNA was collected from mouse MSCs treated with osteogenic and adipogenic stimuli for 3 and 7 days, respectively. Consistently, *Stc1* mRNA levels increased following osteogenic and adipogenic stimulation, with substantially higher expression observed under adipogenic conditions at day 3 (Fig. 1F and G). In addition, *Stc1* expression was examined during chondrogenic differentiation of MSCs, and it was observed that *Stc1* expression remained largely unchanged upon chondrogenic stimulation (Fig. S2A).

Stc1 depletion inhibits senescence and osteogenic differentiation potential of MSCs. Furthermore, it was examined whether *Stc1* depletion affects MSC senescence and lineage specification. Specifically, two siRNAs targeting *Stc1* (si-*Stc1*-1 and si-*Stc1*-2) were used to knock down its expression (Fig. 2A). To minimize off-target effects, the two siRNAs were mixed at a ratio of 1:1 and used for transfection (si-*Stc1*-mix, hereafter referred to as si-*Stc1*). *Stc1* depletion significantly reduced cellular senescence in MSCs, as evidenced by decreased SA-β-Gal staining and downregulated p21 expression, while p16 expression slightly decreased (Fig. S1B-D). Consistently, MSCs exhibited an increased proliferation rate following *Stc1* depletion (Fig. S1E).

ALP staining was performed to assess the effects of *Stc1* knockdown on the osteogenic commitment of MSCs. Notably, ALP activity, an indicator of early osteogenesis, was inhibited by *Stc1* knockdown (Fig. 2B and C). Extracellular matrix mineralization also decreased following *Stc1* knockdown, as determined via ARS staining (Fig. 2D and E). Consistently, the expression levels of osteogenic-related genes were downregulated by *Stc1* knockdown (Fig. 2F). Notably, although *Stc1* was notably upregulated during adipogenesis (39), significant differences were not observed between the *Stc1* knockdown groups and controls in lipid droplet formation or the expression of adipogenic-related genes in MSCs (Fig. 2G-I). In addition, to assess whether STC1 is involved in chondrogenic differentiation, MSCs with STC1 knockdown were subjected to chondrogenic induction and evaluated by multiple readouts, including Alcian blue staining, quantitative glycosaminoglycan (GAG) measurement and expression of chondrogenic marker genes (*Sox9* and *Col2a1*). As shown in Fig. S2B-E, STC1 depletion did not significantly alter matrix deposition, GAG content, or chondrogenic gene expression, indicating that STC1 is dispensable for MSC chondrogenesis under the tested conditions.

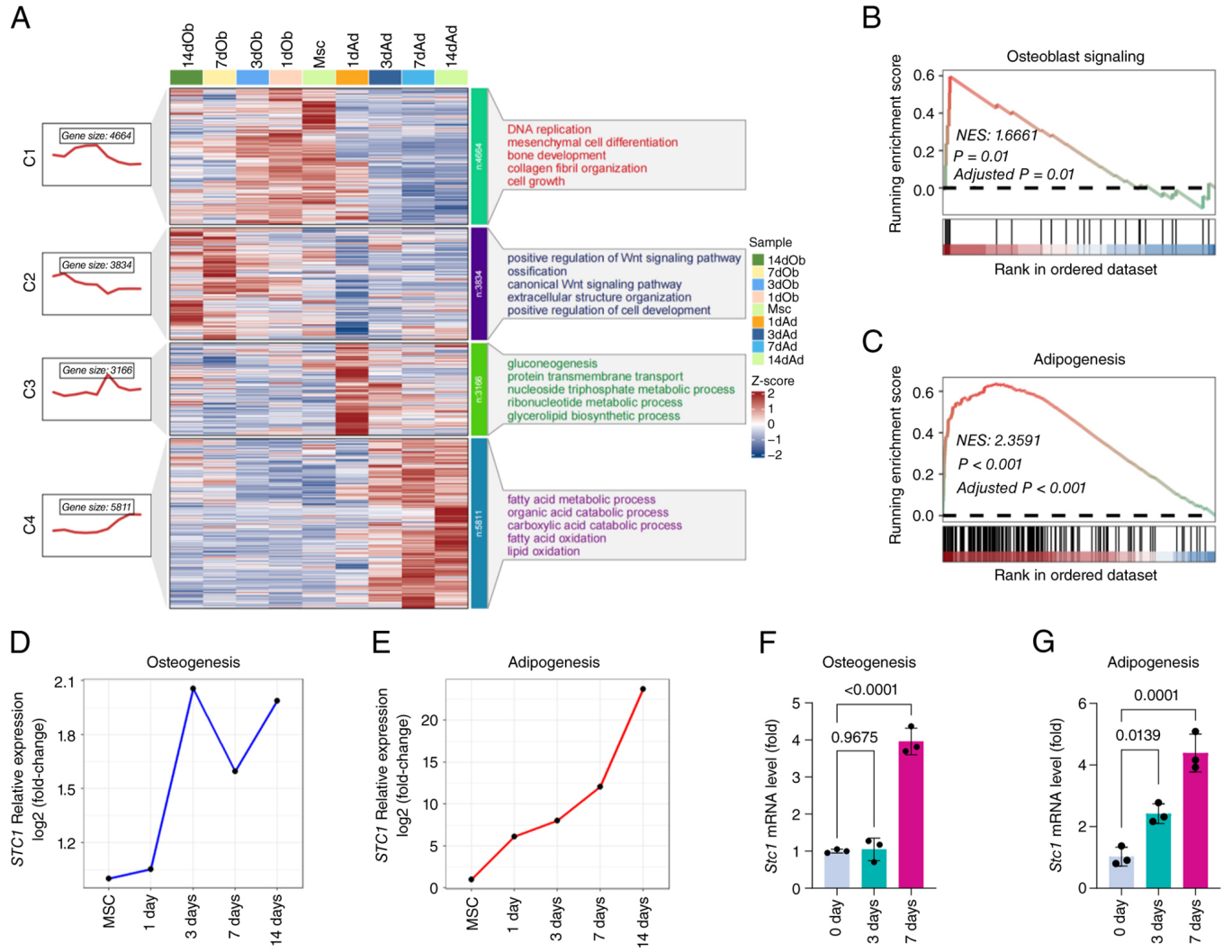

Figure 1. Dynamic transcriptional programs underlying osteogenic and adipogenic differentiation of MSCs. (A) Heatmap showing the expression patterns of differentially expressed genes across MSCs and multiple time points during osteogenic (left) and adipogenic (right) differentiation (1, 3, 7 and 14 d). Differentially expressed genes were grouped into distinct clusters based on their temporal expression trajectories. Functional annotations and representative expression trends for each gene cluster, along with the corresponding gene numbers, are shown on the right. (B) GSEA demonstrating significant enrichment of osteoblast-related signaling pathways during osteogenic differentiation, comparing MSCs with 7-day osteogenic induction. (C) GSEA showing significant enrichment of adipogenesis-related pathways during adipogenic differentiation, comparing MSCs with 7-day adipogenic induction. (D and E) Line plot illustrating the dynamic changes of *STC1* from MSCs upon (D) osteogenic and (E) adipogenic differentiation, respectively. (F and G) *STC1* mRNA levels after 3 and 7 days of (F) osteogenic and (G) adipogenic induction, compared with undifferentiated MSCs. n=3. MSCs, mesenchymal stromal cells; GSEA, gene set enrichment analysis; d, days; STC1, stanniocalcin-1.

Stc1 depletion suppresses osteogenic programs while activating inflammatory signaling. To investigate the effect of *Stc1* knockdown on the transcriptional profile of MSCs, RNA sequencing was performed 3 days after transfection with si-*Stc1* (n=3). PCA revealed a notable separation between control and *Stc1*-depleted MSCs, indicating that *Stc1* knockdown induced a marked global change in gene expression (Fig. 3A). Differential expression analysis identified a total of 3,146 DEGs based on a cutoff of P<0.05 and fold change >1.5, including 1,373 downregulated and 1,773 upregulated genes following *Stc1* knockdown (Fig. 3B). Gene Ontology (GO) enrichment analysis revealed that the downregulated genes were significantly enriched in biological processes related to 'osteogenic differentiation' and 'bone mineralization' (Fig. 3C). By contrast, the upregulated genes were predominantly associated with inflammatory responses, including pathways related to 'interleukin-1 production', 'positive regulation of interleukin-6 production', as well as 'canonical NF-κB signal transduction' (Fig. 3D). GSEA further demonstrated that gene sets associated with osteogenesis and bone mineralization were significantly negatively enriched in *Stc1*-depleted MSCs, whereas gene sets related to inflammatory and immune responses were positively enriched following *Stc1* knockdown (Fig. 3E-H). A heatmap of representative genes further confirmed enhanced inflammatory responses and impaired osteogenic capacity following *Stc1* knockdown (Fig. 3I).

Furthermore, an ATAC-sequencing was performed to examine the impact of *Stc1* depletion on chromatin accessibility in MSCs. Overall, *Stc1* knockdown resulted in only modest changes in global chromatin accessibility (Fig. 4A and B). Differential accessibility analysis identified 4,753 DARs with decreased accessibility and 6,544 DARs with increased

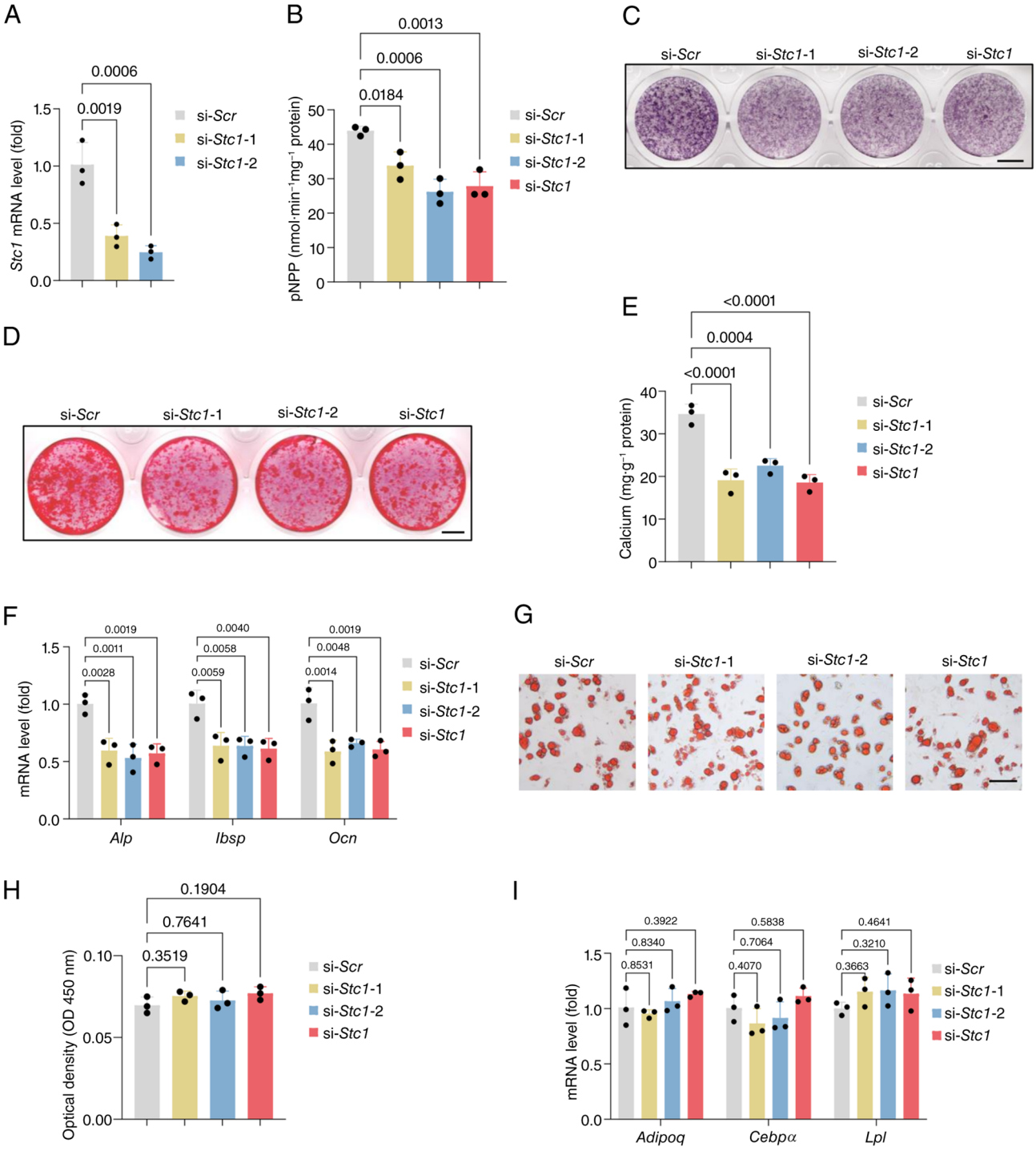

Figure 2. Knockdown of STC1 impairs osteogenic differentiation of MSCs. (A) Relative mRNA level of *Stc1* in MSCs after knockdown of STC1 (n=3). (B and C) ALP staining and quantitative ALP activity assay of MSCs underwent osteogenic induction after knockdown of STC1. Scale bar, 5 mm (n=3). (D and E) ARS staining and quantification of calcium deposit in MSCs underwent osteogenic induction after knockdown of STC1. Scale bar, 5 mm (n=3). (F) mRNA expression of osteogenic marker genes *Alp*, *Ibsp* and *Ocn* in MSCs underwent osteogenic induction after knockdown of STC1 (n=3). (G and H) Oil Red O staining of lipid droplets in MSCs underwent adipogenic induction after knockdown of STC1. Scale bar, 100 μm (n=3). (I) mRNA expression of adipogenic marker genes *Adipoq*, *Cebpα* and *Lpl* in MSCs underwent adipogenic induction after knockdown of STC1 (n=3). MSCs, mesenchymal stromal cells; ALP, alkaline phosphatase; ARS, alizarin red S; STC1, stanniocalcin-1; Scr, scrambled.

accessibility following *Stc1* knockdown, based on a cutoff of P<0.05 (Fig. 4C). Functional annotation of DARs revealed a notable functional divergence between regions gaining or losing accessibility following *Stc1* knockdown. Regions with reduced accessibility were preferentially associated with genes involved in 'collagen-activated signaling pathway', 'regulation of osteoblast differentiation' and 'bone mineralization', indicating selective chromatin closure at osteogenesis-related loci (Fig. 4D). By contrast, regions exhibiting increased accessibility were associated with genes involved in inflammatory processes, including 'interleukin-2 production', 'regulation of canonical NF-κB signal transduction' and 'cell chemotaxis'

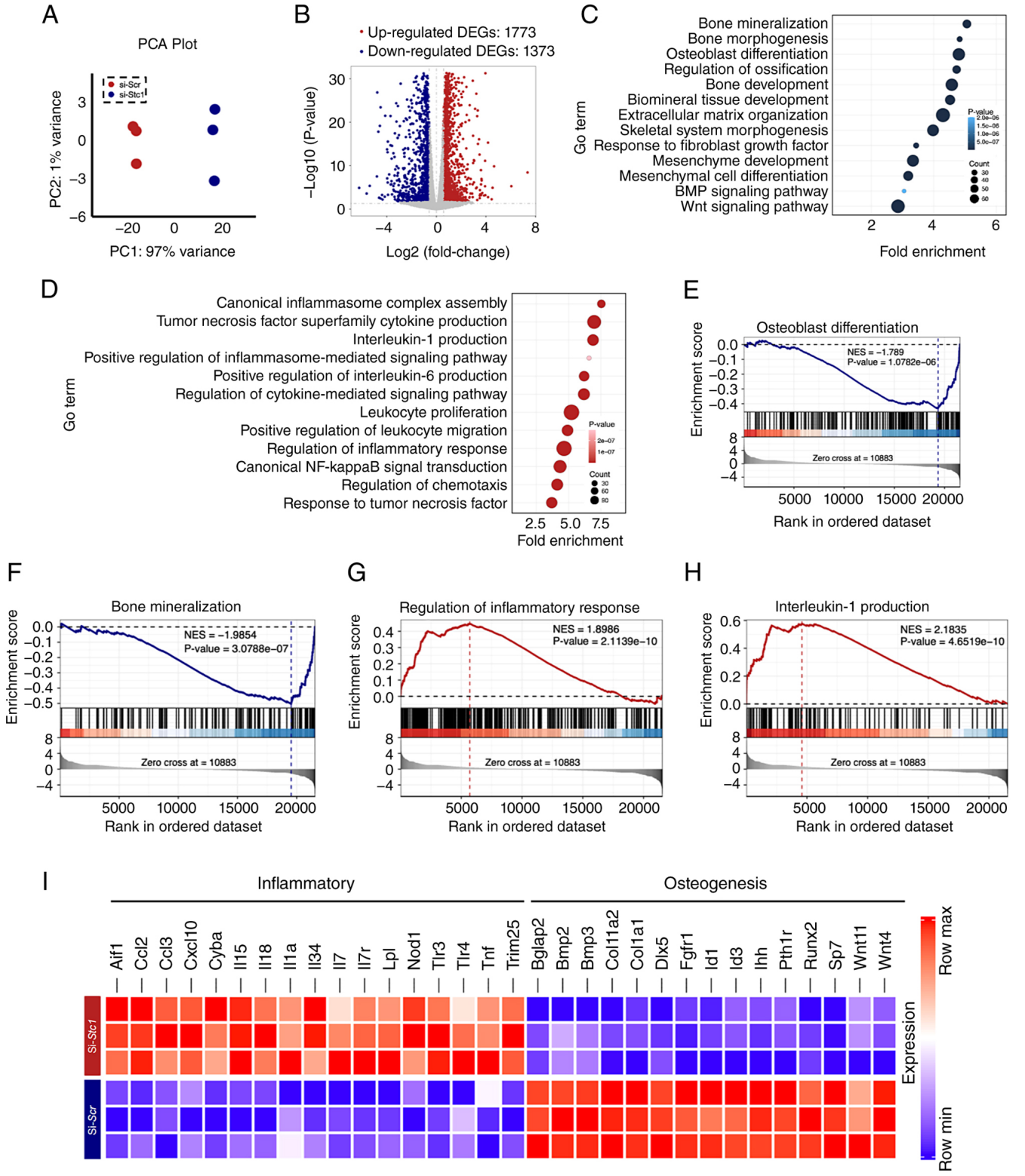

Figure 3. RNA-sequencing analysis of STC1-depleted MSCs. (A) PCA plot showing clear separation between control and STC1-knockdown MSCs. (B) Volcano plot showing differentially expressed genes in MSCs upon STC1 knockdown (fold change >1.5; P<0.05). (C and D) GO enrichment analysis of (C) downregulated or (D) upregulated genes in MSCs underwent STC1 knockdown. (E-H) Gene set enrichment analysis demonstrating negative enrichment of (E and F) osteogenesis-related gene sets and positive enrichment of (G and H) inflammation-related gene sets in STC1-depleted MSCs. (I) Heatmap illustrating enhanced inflammatory response and impaired osteogenesis following STC1 knockdown. MSCs, mesenchymal stromal cells; STC1, stanniocalcin-1; PCA, principal component analysis; DEGs, differentially expressed genes; Scr, scrambled; GO, gene ontology.

(Fig. 4E). Genome track visualization further illustrated these chromatin accessibility changes at representative loci. The promoter regions of osteogenic genes, including *Alp* and *Hoxa3*, exhibited notably reduced accessibility following *Stc1* knockdown (Fig. 4F and G). By contrast, increased chromatin accessibility was observed at the promoters

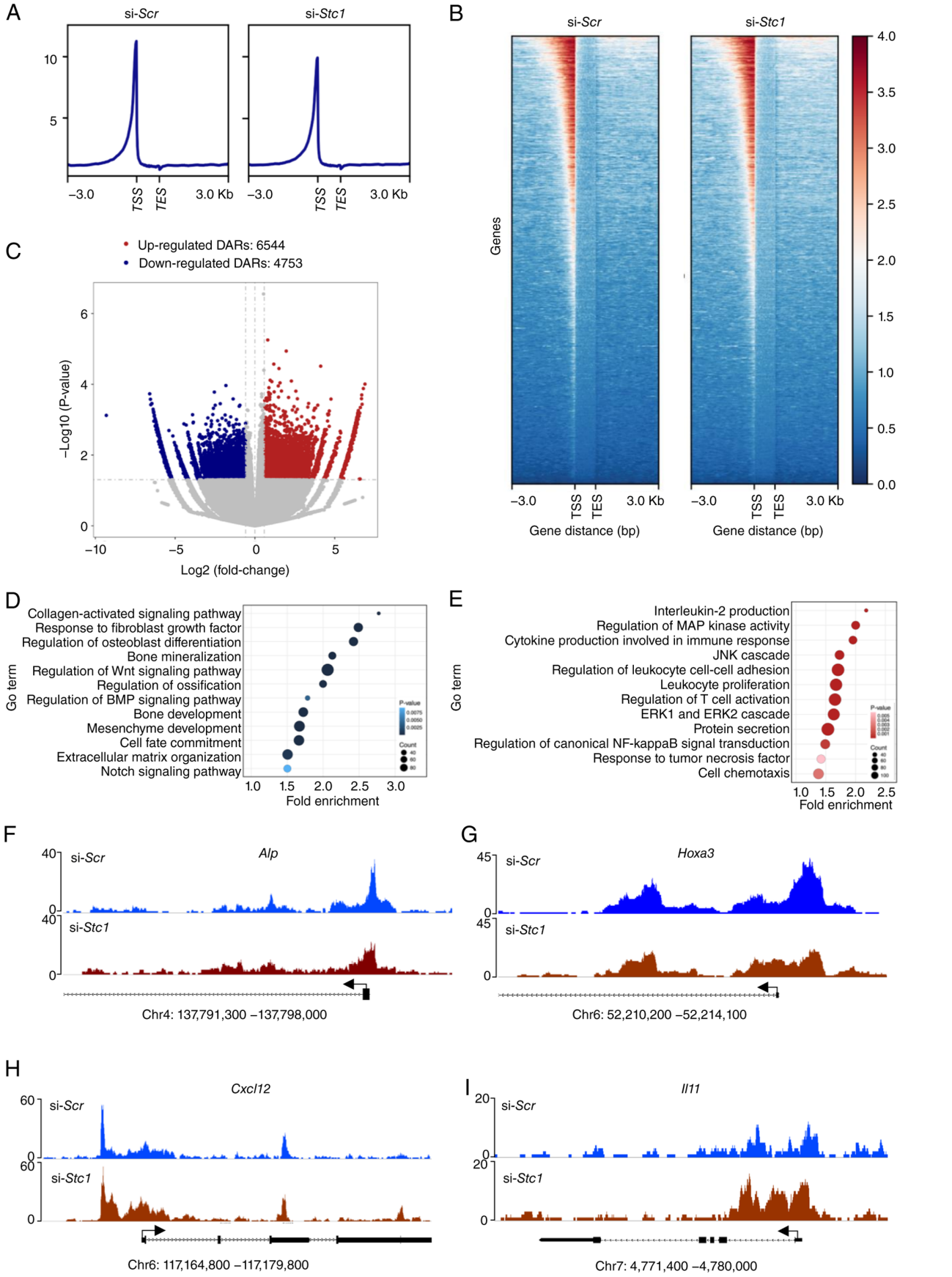

Figure 4. ATAC-sequencing analysis of chromatin accessibility changes upon STC1 knockdown in MSCs. (A and B) Global chromatin accessibility profiles in control and STC1-knockdown MSCs. (C) Numbers of DARs with increased or decreased accessibility upon STC1 knockdown. (D and E) GO terms enriched for genes associated with DARs that (D) lose or (E) gain accessibility upon STC1 knockdown, respectively. (F and G) Genome browser tracks showing reduced chromatin accessibility at the promoter regions of osteogenic genes, such as (F) *Alp* and (G) *Hoxa3*. (H and I) Genome browser tracks showing increased chromatin accessibility at the promoter regions of inflammation-related genes, such as (H) *Cxcl12* and (I) *Il11*. MSCs, mesenchymal stromal cells; STC1, stanniocalcin-1; Scr, scrambled; DARs, differentially accessible regions; GO, gene ontology.

of inflammation-related genes, such as *Cxcl12* and *Il11* (Fig. 4H and I). Collectively, transcriptomic and chromatin accessibility analysis indicated that STC1 knockdown selectively repressed osteogenic programs while concomitantly activating inflammatory pathways.

Stc1 depletion enhancing NF-κB signaling in MSCs. To further elucidate the coordinated transcriptional and chromatin accessibility changes induced by *Stc1* knockdown, an integrative analysis of the RNA-sequencing and ATAC-sequencing datasets was performed. A total of 261 overlapping genes exhibited both decreased transcript abundance in RNA-sequencing and reduced chromatin accessibility in ATAC-sequencing (Fig. 5A). Functional enrichment analysis of this gene set revealed an association with osteogenesis-related processes, including 'bone trabecular formation', 'osteoblast differentiation' and 'skeletal system morphogenesis' (Fig. 5B). Conversely, 374 overlapping genes were identified that exhibited upregulation at the transcript level and increased chromatin accessibility (Fig. 5C). Enrichment analysis of these genes indicated predominant involvement in inflammatory and immune-related pathways, such as 'regulation of interleukin-6 production', 'canonical inflammasome complex assembly' and 'regulation of canonical NF-κB signal transduction' (Fig. 5D). Consistent with the Venn diagram analysis, the integrative heatmap revealed that inflammatory and NF-κB-related genes (including *Tlr4*, *Il6ra*, *Pycard* and *Cxcl12*) were upregulated and exhibited increased chromatin accessibility, whereas osteogenesis-related genes (including *Col1a1*, *Bglap*, *Alpl*, *Smad5* and *Dlx2*) were downregulated and exhibited reduced accessibility (Fig. 5E). These findings indicated that *Stc1* knockdown was associated with coordinated transcriptional and chromatin accessibility changes related to inflammatory activation and impaired osteogenic programs. NF-κB signaling has been well established as a central regulator of MSC osteogenic differentiation and inflammatory responses (40,41). Given the consistent enrichment of inflammatory and NF-κB signaling pathways, it was examined whether *Stc1* knockdown activates NF-κB signaling in MSCs. To further confirm this pathway activation, GSEA was performed on the RNA-sequencing dataset, which revealed significant enrichment of the canonical NF-κB signaling gene set in the *Stc1* knockdown group (Fig. 5F). Western blot analysis revealed a notable increase in p65 phosphorylation, accompanied by a slight increase in phosphorylated IκBα, indicating early activation of canonical NF-κB signaling (Fig. 5G). Consistently, the expression levels of several well-established NF-κB downstream target genes, including *Birc3*, *Icam1*, *Vcam1*, *Tnf* and *Il1α* (42), were significantly upregulated following *Stc1* knockdown (Fig. 5H). Collectively, these results provided molecular evidence that STC1 depletion activates the NF-κB signaling pathway in MSCs.

NF-κB signaling inhibition mitigating impaired osteogenic differentiation of MSCs. To determine whether inhibition of NF-κB signaling could mitigate the impaired osteogenic differentiation induced by *Stc1* knockdown, MSCs were treated with the NF-κB inhibitor BAY 11-7082 (43,44). To exclude potential cytotoxic effects, cell viability was first assessed via a CCK-8 assay. Treatment with BAY 11-7082 at the concentrations used in the present study did not significantly affect MSC viability (Fig. 6A). Consequently, the inhibitory efficiency of BAY 11-7082 was verified via western blot analysis (Fig. 6B). As shown, treatment with BAY 11-7082 markedly reduced the phosphorylation levels of p65 and IκBα. Densitometric analysis revealed that p-p65 and p-IκBα levels were decreased by approximately 60 and 36%, respectively, compared with the control group. By contrast, total p65 and IκBα protein levels remained largely unchanged, indicating effective suppression of NF-κB pathway activation rather than alterations in protein expression. ALP activity assays revealed that treatment with BAY 11-7082 at concentrations of 1 and 2 μM increased ALP activity during osteogenic differentiation of MSCs (Fig. 6C and D). Consistent with this observation, ARS staining revealed that BAY 11-7082 treatment effectively mitigated the reduction in extracellular matrix mineralization induced by *Stc1* depletion (Fig. 6E and F). Moreover, the expression levels of osteogenic marker genes, *Alp* and *Ocn*, exhibited a similar increasing trend following BAY 11-7082 treatment (Fig. 6G and H).

To further validate these findings, MSCs were treated with JSH-23, an alternative NF-κB inhibitor, at concentrations of 20 and 50 μM during osteogenic induction (44). To exclude potential cytotoxic effects, cell viability was first assessed via a CCK-8 assay, which demonstrated that JSH-23 at 20 and 50 μM did not significantly affect MSC viability (Fig. S3A). Similar to BAY 11-7082, JSH-23 treatment enhanced osteogenic differentiation and restored osteogenic capacity in *Stc1*-knockdown MSCs (Fig. S3B-G). Overall, following treatment with either BAY 11-7082 or JSH-23, osteogenic differentiation in *Stc1*-depleted MSCs reached or even exceeded that observed in scrambled siRNA control cells treated with vehicle, indicating a robust mitigating effect.

Given the essential role of NF-κB in the regulation of inflammation, BAY 11-7082 treatment was expected to inhibit the expression of inflammatory factors, *Il1a* and *Tnf*, induced by *Stc1* depletion. Notably, treatment with 2 μM BAY 11-7082 reduced their expression (Fig. 6I and J). Inhibition of NF-κB signaling by BAY 11-7082 further enhanced the effect of *Stc1* depletion on cellular senescence, as evidenced by the SA-β-gal assay (Fig. 6K and L). Similarly, treatment with JSH-23 also inhibited the expression of *Il1a* and *Tnfa* and further mitigated senescence in STC1-depleted MSCs (Fig. S3H-K).

Collectively, these results identify STC1 as a key regulator of osteogenic differentiation and inflammation in MSCs. These findings provide mechanistic insight into the role of STC1 in MSC biology and highlight that modulation of STC1 and NF-κB signaling requires further investigation in more physiologically relevant and *in vivo* models of age-related bone loss.

Discussion

Age-related bone loss represents a major global health challenge in aging societies, leading to increased fracture risk, disability and mortality. Accumulating evidence indicates that the functional decline of MSCs, encompassing reduced cell number, increased cellular senescence, and impaired osteogenic differentiation, is a key contributor to age-related bone loss (3-5). In the present study, it was demonstrated that

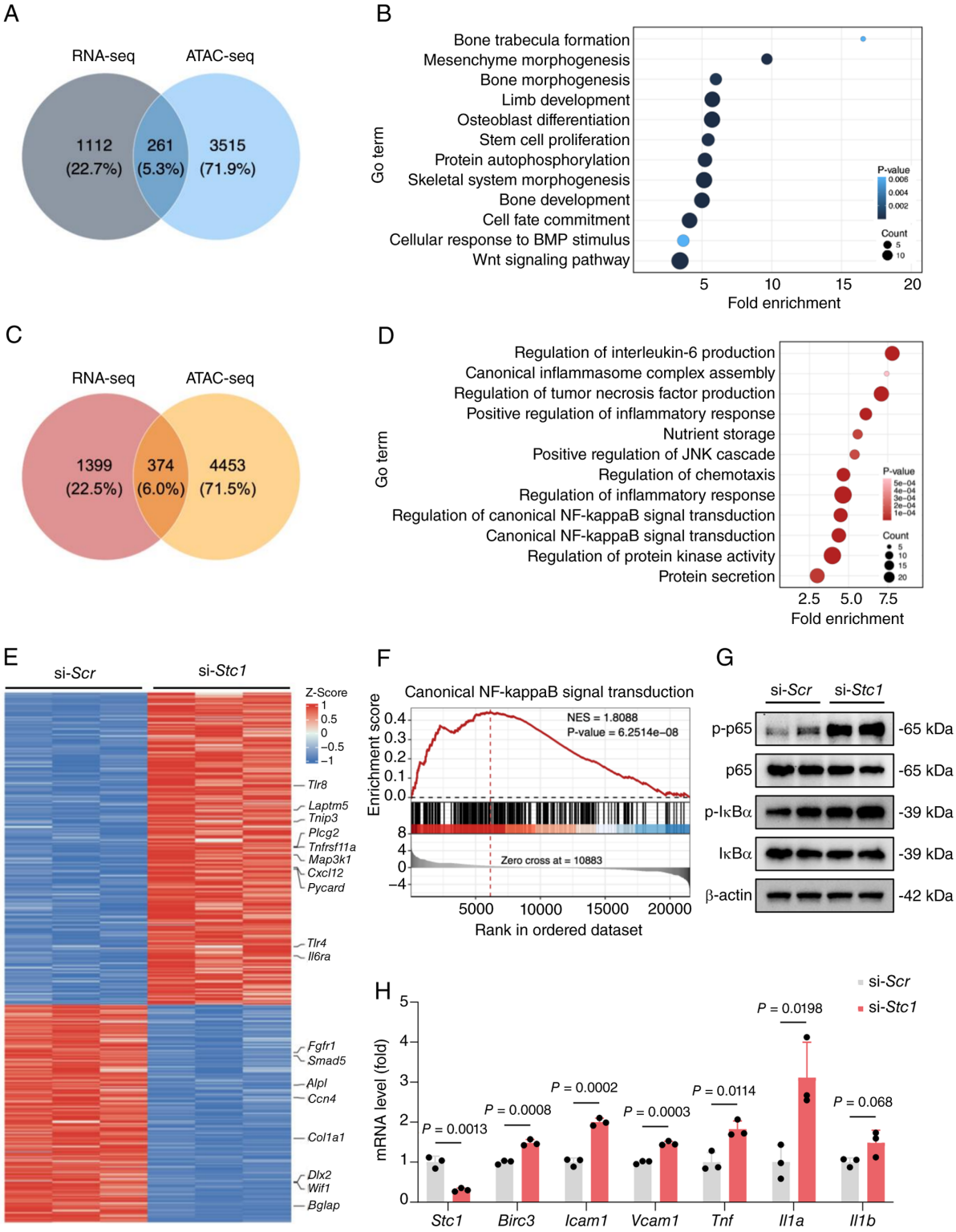

Figure 5. STC1 knockdown activates NF-κB signaling in MSCs. (A) Venn diagram showing the overlap among genes downregulated in RNA-seq, genes associated with decreased chromatin accessibility identified by ATAC-seq. (B) GO analysis of the overlapped genes in (A). (C) Venn diagram showing the overlap among genes upregulated in RNA-seq, genes associated with increased chromatin accessibility identified by ATAC-seq. (D) GO analysis of the overlapped genes in (C). (E) Integrative heatmap of overlapping genes with concordant RNA-seq and ATAC-seq changes. (F) GSEA showing significant enrichment of the NF-κB signaling pathway upon STC1 knockdown. (G) Western blot assay for p-p65, p65 p-IκBα and IκBα protein expression in MSCs following STC1 knockdown. (H) RNA-seq analysis based on FPM values showing upregulation of NF-κB downstream target genes following STC1 knockdown (n=3). Seq, sequencing; MSCs, mesenchymal stromal cells; STC1, stanniocalcin-1; GO, gene ontology.

Stc1 expression is high in aged MSCs and that *Stc1* depletion attenuates MSC senescence. Although *Stc1* upregulation in aged MSCs may reflect a stress-adaptive response, the present results indicate that targeting STC1 represents a potential strategy for modulating MSC senescence and mitigating age-related bone loss.

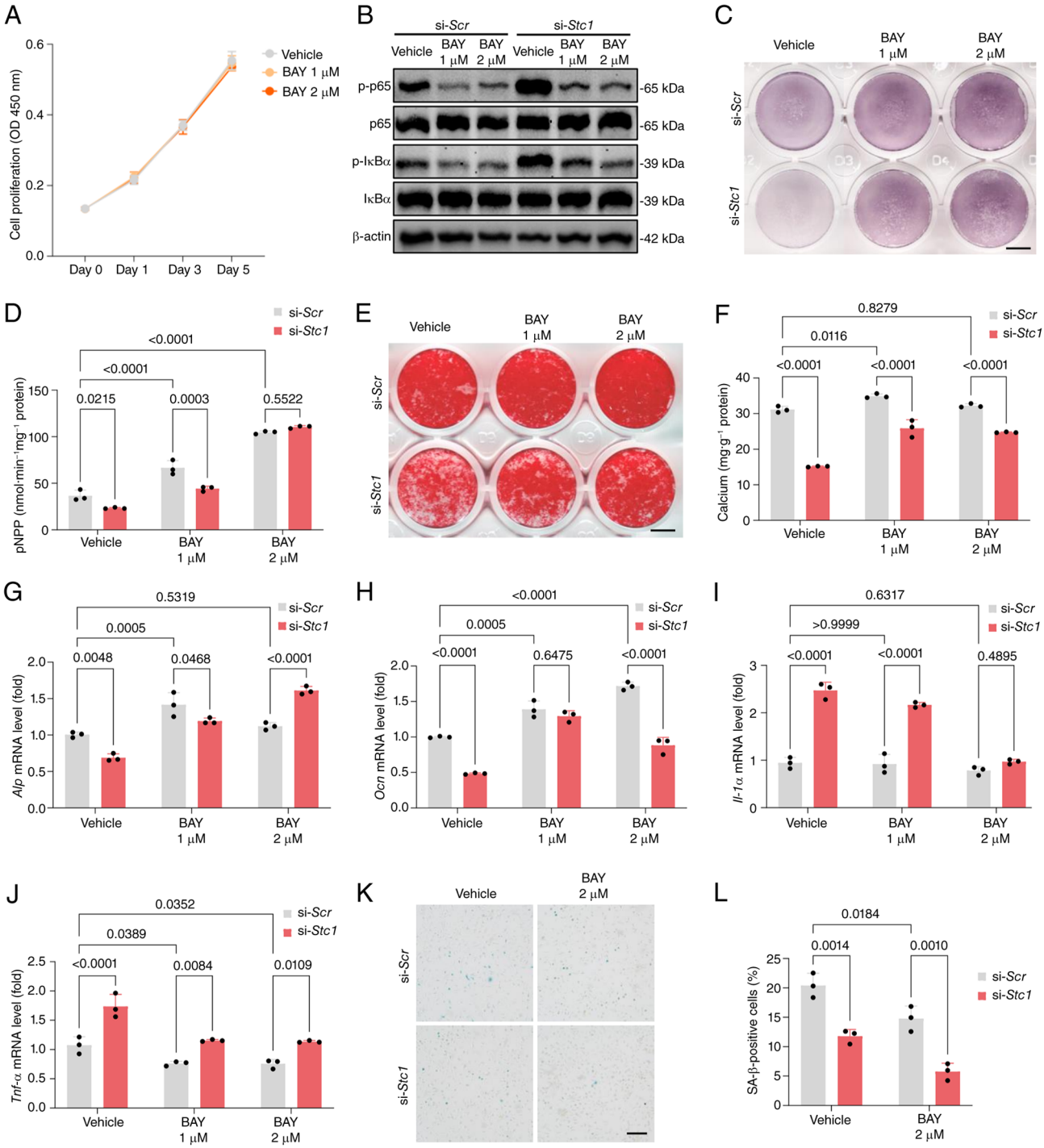

Figure 6. STC1 knockdown and NF-κB inhibition by BAY11-7082 promotes functional rejuvenation of MSCs. (A) Cell counting kit 8 assay of MSCs treated with vehicle or BAY 11-7082 (1 and 2 μM; n=3. (B) Western blot assay for p-p65, p65 p-IκBα and IκBα protein expression in STC1-depleted MSCs treated with vehicle or BAY 11-7082 (1 and 2 μM). (C and D) ALP staining and quantitative ALP activity assay of STC1-knockdown MSCs treated with vehicle or BAY 11-7082 (1 and 2 μM) upon osteogenic induction. Scale bar, 5 mm (n=3). (E and F) ARS staining and quantification of extracellular matrix mineralization in STC1-depleted MSCs treated with vehicle or BAY 11-7082 (1 and 2 μM) upon osteogenic induction. Scale bar, 5 mm (n=3). (G and H) mRNA expression levels of osteogenic marker genes (G) *Alp* and (H) *Ocn* in STC1-depleted MSCs treated with vehicle or BAY 11-7082 (1 and 2 μM) upon osteogenic induction. n=3. (J and K) mRNA expression levels of NF-κB downstream target genes (I) *Il-1α* and (J) *Tnf-α* in STC1-depleted MSCs treated with vehicle or BAY 11-7082 (1 and 2 μM). n=3. (K and L) SA-β-Gal staining and the quantitation of positive cells in STC1-depleted MSCs, after treatment with vehicle, BAY 11-7082 (1 or 2 μM). Scale bar, 200 μm. n=3. BAY, BAY11-7082; MSCs, mesenchymal stromal cells; STC1, stanniocalcin-1; ALP, alkaline phosphatase; ARS, alizarin red S; Scr, scrambled; SA-β-Gal, senescence associate β-galactosidase.

Previous studies have reported both activating and suppressing effects of STC1 on NF-κB signaling, depending on tissue context and disease state. For example, STC1 has been shown to regulate ROS homeostasis and inflammatory responses in mesenchymal stromal cells, macrophages and lung cancer models (27,28). In MSCs, it was observed in the present study that STC1 depletion results in robust activation of NF-κB signaling, accompanied by increased expression of

downstream inflammatory target genes. These results indicate that the regulatory relationship between STC1 and NF-κB is cell- and context-dependent. Specifically, STC1 influences NF-κB activity indirectly through regulation of intracellular redox homeostasis, as STC1 has been shown to modulate ROS production in multiple cell types (27,28). Notably, pharmacological inhibition of NF-κB signaling mitigated the osteogenic defects induced by STC1 knockdown, indicating that NF-κB signaling is possibly involved in mediating the effects of STC1 depletion on MSC osteogenic potential.

Chronic low-grade inflammation is increasingly recognized as a hallmark and driving force of aging across multiple tissues (11,12). In the skeletal system, inflammatory signaling accelerates bone resorption and suppresses MSC osteogenic differentiation. Senescent MSCs exhibit a pro-inflammatory secretory phenotype enriched in cytokines and chemokines such as IL-1α, IL-6 and CXCL family members, which further exacerbate tissue dysfunction (6,7). STC1 has been reported to modulate inflammatory responses in diverse biological contexts (25-28). Notably, it was observed in the present study that STC1 depletion in MSCs leads to activation of inflammatory genes, indicating a previously unrecognized anti-inflammatory role of STC1 in this cell type. The ability of NF-κB inhibition to rescue osteogenic differentiation in STC1-deficient MSCs may therefore be attributed, at least in part, to suppression of inflammation-associated inhibitory signals. Notably, while STC1 knockdown attenuated certain senescence-associated phenotypes in MSCs, it concurrently suppressed osteogenic programs and activated inflammatory/NF-κB signaling. In this context, the inhibitory effects on osteogenic differentiation outweighed the potential benefits of reduced senescence. These results suggest that in MSCs, regulation of senescence and osteogenesis are not necessarily coupled processes, highlighting the complex role of STC1 in coordinating cellular fate.

Furthermore, the role of STC1 appears to be notably cell type- and context-dependent. Previous studies investigating STC1 in bone biology largely focused on mature osteoblasts, osteocytes or chondrocytes, where STC1 has been reported to exert either promotive or inhibitory effects on osteogenic activity (20-24). For example, STC1 has been reported to inhibit longitudinal bone growth in growth plate chondrocytes (20) and to negatively regulate osteoblast differentiation and bone formation in transgenic mouse bone marrow-derived MSCs (24). By contrast, STC1 has been shown to promote osteogenic differentiation in human MSCs (45) and dental follicle cells (46) and to contribute to bone-protective effects in pathological settings such as CCl4-induced bone loss (47). MSCs are notably responsive to inflammatory and senescence-associated cues, and their lineage commitment is markedly regulated by the balance between osteogenic and inflammatory signaling pathways (40,48). Emerging evidence also suggests that MSC-derived STC1 participates in stress adaptation and immunomodulatory signaling in several disease models (25-27). The present findings reveal that, in MSCs, STC1 mainly functions as a suppressor of NF-κB-associated inflammatory signaling and a maintainer of osteogenic potential. Therefore, the effects of STC1 observed in differentiated bone cells may not fully reflect its regulatory role in MSC fate determination during aging. These observations further highlight the functional heterogeneity of STC1 across different cell types and indicate that the biological effects of STC1 should be interpreted within a specific cellular and developmental context.

From a therapeutic perspective, modulation of STC1 in MSCs may represent a potential strategy for improving osteogenic capacity under inflammatory conditions. This improvement can theoretically be achieved through localized delivery approaches, such as bone-targeted gene or mRNA delivery systems. However, STC1 is widely expressed in multiple tissues as a secreted protein, which raises concerns regarding target specificity and potential off-target effects. Therefore, any future therapeutic application would require precise spatial control of STC1 activity within the bone marrow niche.

Finally, several limitations of the present study should be acknowledged. First, all experiments were performed using cultured MSCs *in vitro*. Therefore, the physiological relevance of these findings *in vivo* is yet to be established. In addition, although the present data support the involvement of NF-κB signaling following STC1 depletion, the precise molecular mechanisms associating STC1 with NF-κB activation require further investigation. Furthermore, future studies using *in vivo* or *ex vivo* osteoporotic models may further clarify the role of STC1 in the bone microenvironment and assess its potential relevance in age-related bone loss.

In summary, the present study revealed a novel role of STC1 in coordinating cellular senescence, inflammation, and osteogenic differentiation in MSCs. By inhibiting NF-κB activation, STC1 preserves osteogenic potential and limits inflammation-driven lineage imbalance.

Acknowledgements

Not applicable.

Funding

The present study was supported by the National Natural Science Foundation of China (grant nos. 82370918, U25A6003, 82571774 and 82301074), Department of Science and Technology of Zhejiang Province (grant nos. 2024C03193 and 2025C02100) and the Sichuan Science and Technology Program (grant no. 2026YFHZ0149).

Availability of data and materials

All sequencing data in the present study are available at National Genomics Data Center, China National Center for Bioinformation under the accession number CRA038035 (https://ngdc.cncb.ac.cn/gsa/browse/CRA038035). All other data generated in the present study may be requested from the corresponding author.

Author's contributions

LF, PD and QMC conceived the present study. LF, PD, QMC, XC and XX designed the experiments. CY, XL, PW, YC, EW, QC, JH, FZ, LG, JL, MZ, JZ, BH, AAB, YM, JKK, IC, JC, PHK and LH performed the experiments. CY, XL, PW and EW performed the data analysis. CY, XL, XC, PD and QMC wrote the manuscript. All authors confirm the authenticity of

all the raw data, and read and approved the final version of the manuscript.

Ethics approval and consent to participate

All procedures were performed according to established ethical guidelines and approved by the Institutional Animal Care and Use Committee of Zhejiang University (approval nos. ZJU20230513 and ZJU20240033).

Patient consent for publication

Not applicable.

Competing interests

The authors declare that they have no competing interests.

References

1. Zhou J and Shi Y: Mesenchymal stem/stromal cells (MSCs): Origin, immune regulation, and clinical applications. Cell Mol Immunol 20: 555-557, 2023.
2. Bianco P, Cao X, Frenette PS, Mao JJ, Robey PG, Simmons PJ and Wang CY: The meaning, the sense and the significance: Translating the science of mesenchymal stem cells into medicine. Nat Med 19: 35-42, 2013.
3. Zhang L, Wang Z, Zhang Y, Ji R, Li Z, Zou J and Gao B: Regulatory cellular and molecular networks in the bone microenvironment during aging. Life Med 3: nae019, 2024.
4. Deng P, Yuan Q, Cheng Y, Li J, Liu Z, Liu Y, Li Y, Su T, Wang J, Salvo ME, *et al*: Loss of KDM4B exacerbates bone-fat imbalance and mesenchymal stromal cell exhaustion in skeletal aging. Cell Stem Cell 28: 1057-1073.e7, 2021.
5. Cheng M, Yuan W, Moshaverinia A and Yu B: Rejuvenation of mesenchymal stem cells to ameliorate skeletal aging. Cells 12: 998, 2023.
6. Gnani D, Crippa S, Della Volpe L, Rossella V, Conti A, Lettera E, Rivis S, Ometti M, Fraschini G, Bernardo ME and Di Micco R: An early-senescence state in aged mesenchymal stromal cells contributes to hematopoietic stem and progenitor cell clonogenic impairment through the activation of a pro-inflammatory program. Aging Cell 18: e12933, 2019.
7. Wang B, Han J, Elisseeff JH and Demaria M: The senescence-associated secretory phenotype and its physiological and pathological implications. Nat Rev Mol Cell Biol 25: 958-978, 2024.
8. Vono R, Jover Garcia E, Spinetti G and Madeddu P: Oxidative stress in mesenchymal stem cell senescence: Regulation by coding and noncoding RNAs. Antioxid Redox Signal 29: 864-879, 2018.
9. Choo KB, Tai L, Hymavathee KS, Wong CY, Nguyen PN, Huang CJ, Cheong SK and Kamarul T: Oxidative Stress-induced premature senescence in Wharton's Jelly-derived mesenchymal stem cells. Int J Med Sci 11: 1201-1207, 2014.
10. Finkel T and Holbrook NJ: Oxidants, oxidative stress and the biology of ageing. Nature 408: 239-247, 2000.
11. Baechle JJ, Chen N, Makhijani P, Winer S, Furman D and Winer DA: Chronic inflammation and the hallmarks of aging. Mol Metab 74: 101755, 2023.
12. Andonian BJ, Hippensteel JA, Abuabara K, Boyle EM, Colbert JF, Devinney MJ, Faye AS, Kochar B, Lee J, Litke R, *et al*: Inflammation and aging-related disease: A transdisciplinary inflammaging framework. Geroscience 47: 515-542, 2025.
13. De Cecco M, Ito T, Petrashen AP, Elias AE, Skvir NJ, Criscione SW, Caligiana A, Brocculi G, Adney EM, Boeke JD, *et al*: L1 drives IFN in senescent cells and promotes age-associated inflammation. Nature 566: 73-78, 2019.
14. Liu X, Liu Z, Wu Z, Ren J, Fan Y, Sun L, Cao G, Niu Y, Zhang B, Ji Q, *et al*: Resurrection of endogenous retroviruses during aging reinforces senescence. Cell 186: 287-304.e26, 2023.
15. Yang JH, Hayano M, Griffin PT, Amorim JA, Bonkowski MS, Apostolides JK, Salfati EL, Blanchette M, Munding EM, Bhakta M, *et al*: Loss of epigenetic information as a cause of mammalian aging. Cell 186: 305-326.e27, 2023.
16. Kløverpris S, Mikkelsen JH, Pedersen JH, Jepsen MR, Laursen LS, Petersen SV and Oxvig C: Stanniocalcin-1 Potently inhibits the proteolytic activity of the metalloproteinase Pregnancy-associated plasma Protein-A. J Biol Chem 290: 21915-21924, 2015.
17. Basisty N, Kale A, Jeon OH, Kuehnemann C, Payne T, Rao C, Holtz A, Shah S, Sharma V, Ferrucci L, *et al*: A proteomic atlas of senescence-associated secretomes for aging biomarker development. PLoS Biol 18: e3000599, 2020.
18. Zhu L, Xie Z, Yang G, Zhou G, Li L and Zhang S: Stanniocalcin-1 Promotes PARP1-Dependent cell death via JNK activation in colitis. Adv Sci (Weinh) 11: e2304123, 2024.
19. Yoshiko Y, Son A, Maeda S, Igarashi A, Takano S, Hu J and Maeda N: Evidence for stanniocalcin gene expression in mammalian bone. Endocrinology 140: 1869-1874, 1999.
20. Wu S, Yoshiko Y and De Luca F: Stanniocalcin 1 acts as a paracrine regulator of growth plate chondrogenesis. J Biol Chem 281: 5120-5127, 2006.
21. Filvaroff EH, Guillet S, Zlot C, Bao M, Ingle G, Steinmetz H, Hoeffel J, Bunting S, Ross J, Carano RA, *et al*: Stanniocalcin 1 alters muscle and bone structure and function in transgenic mice. Endocrinology 143: 3681-3690, 2002.
22. Varghese R, Gagliardi AD, Bialek PE, Yee SP, Wagner GF and Dimattia GE: Overexpression of human stanniocalcin affects growth and reproduction in transgenic mice. Endocrinology 143: 868-876, 2002.
23. Yoshiko Y, Maeda N and Aubin JE: Stanniocalcin 1 stimulates osteoblast differentiation in rat calvaria cell cultures. Endocrinology 144: 4134-4143, 2003.
24. Kim JH, Kim K, Kim I, Seong S, Koh JT and Kim N: Stanniocalcin 1 and 1,25-dihydroxyvitamin D3 cooperatively regulate bone mineralization by osteoblasts. Exp Mol Med 56: 1991-2001, 2024.
25. Zonderland J, Gomes DB, Pallada Y, Moldero IL, Camarero-Espinosa S and Moroni L: Mechanosensitive regulation of stanniocalcin-1 by zyxin and actin-myosin in human mesenchymal stromal cells. Stem Cells 38: 948-959, 2020.
26. Bartosh TJ, Ylöstalo JH, Bazhanov N, Kuhlman J and Prockop DJ: Dynamic compaction of human mesenchymal stem/precursor cells into spheres self-activates caspase-dependent IL1 signaling to enhance secretion of modulators of inflammation and immunity (PGE2, TSG6, and STC1). Stem Cells 31: 2443-2456, 2013.
27. Seo Y, Shin TH, Ahn JS, Oh SJ, Shin YY, Yang JW, Park HY, Shin SC, Kwon HK, Kim JM, *et al*: Human Tonsil-derived mesenchymal stromal cells maintain proliferating and ROS-Regulatory properties via Stanniocalcin-1. Cells 9: 636, 2020.
28. Ohkouchi S, Block GJ, Katsha AM, Kanehira M, Ebina M, Kikuchi T, Saijo Y, Nukiwa T and Prockop DJ: Mesenchymal stromal cells protect cancer cells from ROS-induced apoptosis and enhance the Warburg effect by secreting STC1. Mol Ther 20: 417-423, 2012.
29. Deng P, Chang I, Wang J, Badreldin AA, Li X, Yu B and Wang CY: Loss of KDM4B impairs osteogenic differentiation of OMSCs and promotes oral bone aging. Int J Oral Sci 14: 24, 2022.
30. Liu Z, Lee HL, Suh JS, Deng P, Lee CR, Bezouglaia O, Mirnia M, Chen V, Zhou M, Cui ZK, *et al*: The ERα/KDM6B regulatory axis modulates osteogenic differentiation in human mesenchymal stem cells. Bone Res 10: 3, 2022.
31. Zhu M, Min S, Mao X, Zhou Y, Zhang Y, Li W, Li L, Wu L, Cong X and Yu G: Interleukin-13 promotes cellular senescence through inducing mitochondrial dysfunction in IgG4-related sialadenitis. Int J Oral Sci 14: 29, 2022.
32. Livak KJ and Schmittgen TD: Analysis of relative gene expression data using real-time quantitative PCR and the 2(-Delta Delta C(T)) method. Methods 25: 402-408, 2001.
33. Dobin A, Davis CA, Schlesinger F, Drenkow J, Zaleski C, Jha S, Batut P, Chaisson M and Gingeras TR: STAR: Ultrafast universal RNA-seq aligner. Bioinformatics 29: 15-21, 2012.
34. Liao Y, Smyth GK and Shi W: featureCounts: An efficient general purpose program for assigning sequence reads to genomic features. Bioinformatics 30: 923-930, 2013.
35. Rauch A, Haakonsson AK, Madsen JGS, Larsen M, Forss I, Madsen MR, Van Hauwaert EL, Wiwie C, Jespersen NZ, Tencerova M, *et al*: Osteogenesis depends on commissioning of a network of stem cell transcription factors that act as repressors of adipogenesis. Nat Genet 51: 716-727, 2019.

36. Wang C, Tian W, Hu SY, Di CX, He CY, Cao QL, Hao RH, Dong SS, Liu CC, Rong Y, *et al*: Lineage-selective super enhancers mediate core regulatory circuitry during adipogenic and osteogenic differentiation of human mesenchymal stem cells. Cell Death Dis 13: 866, 2022.
37. Langmead B and Salzberg SL: Fast gapped-read alignment with Bowtie 2. Nat Methods 9: 357-359, 2012.
38. Zhang Y, Liu T, Meyer CA, Eeckhoute J, Johnson DS, Bernstein BE, Nusbaum C, Myers RM, Brown M, Li W and Liu XS: Model-based analysis of ChIP-Seq (MACS). Genome Biol 9: R137, 2008.
39. Serlachius M and Andersson LC: Upregulated expression of stanniocalcin-1 during adipogenesis. Exp Cell Res 296: 256-264, 2004.
40. Chang J, Liu F, Lee M, Wu B, Ting K, Zara JN, Soo C, Al Hezaimi K, Zou W, Chen X, *et al*: NF-κB inhibits osteogenic differentiation of mesenchymal stem cells by promoting β-catenin degradation. Proc Natl Acad Sci USA 110: 9469-9474, 2013.
41. Wang L, Zhao Y, Liu Y, Akiyama K, Chen C, Qu C, Jin Y and Shi S: IFN-γ and TNF-α synergistically induce mesenchymal stem cell impairment and tumorigenesis via NFκB signaling. Stem Cells 31: 1383-1395, 2013.
42. Guo Q, Jin Y, Chen X, Ye X, Shen X, Lin M, Zeng C, Zhou T and Zhang J: NF-κB in biology and targeted therapy: New insights and translational implications. Signal Transduct Target Ther 9: 53, 2024.
43. Hou Y, Liang H, Rao E, Zheng W, Huang X, Deng L, Zhang Y, Yu X, Xu M, Mauceri H, *et al*: Non-canonical NF-κB Antagonizes STING Sensor-Mediated DNA sensing in radiotherapy. Immunity 49: 490-503.e4, 2018.
44. Mori N, Yamada Y, Ikeda S, Yamasaki Y, Tsukasaki K, Tanaka Y, Tomonaga M, Yamamoto N and Fujii M: Bay 11-7082 inhibits transcription factor NF-kappaB and induces apoptosis of HTLV-I-infected T-cell lines and primary adult T-cell leukemia cells. Blood 100: 1828-1834, 2002.
45. Brum AM, van de Peppel J, Nguyen L, Aliev A, Schreuders-Koedam M, Gajadien T, van der Leije CS, van Kerkwijk A, Eijken M, van Leeuwen JPTM and van der Eerden BCJ: Using the Connectivity Map to discover compounds influencing human osteoblast differentiation. J Cell Physiol 233: 4895-4906, 2018.
46. Felthaus O, Gosau M and Morsczeck C: ZBTB16 induces osteogenic differentiation marker genes in dental follicle cells independent from RUNX2. J Periodontol 85: e144-e151, 2014.
47. Sonoda S, Murata S, Yamaza H, Yuniartha R, Fujiyoshi J, Yoshimaru K, Matsuura T, Oda Y, Ohga S, Tajiri T, *et al*: Targeting hepatic oxidative stress rescues bone loss in liver fibrosis. Mol Metab 66: 101599, 2022.
48. Deshpande S, James AW, Blough J, Donneys A, Wang SC, Cederna PS, Buchman SR and Levi B: Reconciling the effects of inflammatory cytokines on mesenchymal cell osteogenic differentiation. J Surg Res 185: 278-285, 2013.